CSIRO PUBLISHING

Exploration Geophysics, 2015, **46**, 153–158
http://dx.doi.org/10.1071/EG13061

Gaussian beam prestack depth migration in heterogeneous transversely isotropic media

Jianguang Han[1,2] Yun Wang[3,4]

[1]Institute of Geology and Geophysics, Chinese Academy of Sciences, Beijing 100029, China.
[2]University of Chinese Academy of Sciences, Beijing 100049, China.
[3]Institute of Geochemistry, Chinese Academy of Sciences, Guiyang 550002, China.
[4]Corresponding author. Email: yunwang@mail.iggcas.ac.cn

Abstract. The transversely isotropic (TI) media approximation is commonly applied to assist in the processing of seismic data acquired in sedimentary environments. Based on anisotropic kinematic and dynamic ray tracing systems, a P-wave Gaussian beam prestack depth migration (GB-PSDM) method for TI media is introduced in this paper. The imaging principle of anisotropic GB-PSDM and the corresponding migration parameters are presented on the basis of the GB-PSDM method in isotropic media. Tests of synthetic and field seismic data show that the method is an accurate and efficient anisotropic prestack depth migration method in TI media.

Key words: anisotropy, Gaussian beam prestack depth migration, ray tracing, transversely isotropy media.

Received 23 June 2013, accepted 17 February 2014, published online 18 March 2014

Introduction

Depth migration is one of the most effective seismic techniques for imaging complex subsurface structures. Migration algorithms are usually divided into two classes: ray-based Kirchhoff migration and wave-equation migration. For these migration methods, the ray-based Kirchhoff method is more efficient and flexible, but it has the phenomena of multi-valued traveltimes which affects migration results. The wave-equation migration can provide more accurate images. However, the method is very time consuming. Gaussian beam migration, as a powerful imaging technique, is an elegant and efficient depth migration method, with accuracy comparable to wave-equation migration and flexibility comparable to Kirchhoff migration (Gray and Bleistein, 2009).

At present, the Gaussian beam migration research is studied mainly in isotropic media. Hill (1990) first proposed a Gaussian beam poststack migration method and did a detailed study on migration parameters. Hale (1992*a*, 1992*b*) further introduced algorithm and implementation of Gaussian beam migration. Hill (2001) presented a prestack Gaussian beam migration method in isotropic media which operates on common-offset and common-azimuth data volumes. Gray (2005) removed the narrow azimuth restriction by presenting variations suitable for common-shot records migration. In further publications, true-amplitude Gaussian-beam migration methods in isotropic media were developed by Gray and Bleistein (2009) and Popov et al. (2008, 2010).

However, it has been shown by previous studies (Ball, 1995; Wang, 2002) that seismic anisotropy widely exists in the subsurface media. Failure to account for anisotropy in migration algorithms may lead to large positional errors or a complete loss of steeply dipping structures (Zhang et al., 2001). Therefore, to obtain accurate seismic images of subsurface structures, the anisotropy cannot be ignored in migration processing. Since the transversely isotropic (TI) approximation is one of the most common and practical approximations for anisotropic media, and most sedimentary rocks can be described as being TI with a symmetry-axis perpendicular to the bedding plane (Pedersen et al., 2010), it is of great significance to study the migration algorithm in TI media, which can eliminate the influence of anisotropy and realise accurate images of subsurface structures. Gaussian beam migration for anisotropy has been developed in the past few years. Alkhalifah (1995) first proposed a Gaussian beam poststack depth migration method for anisotropic media. Zhu et al. (2007) presented a prestack Gaussian beam depth migration method in anisotropic media and applied it with encouraging results to synthetic data.

Based on the study of Gaussian beam poststack depth migration for anisotropic media (Alkhalifah, 1995), an anisotropic Gaussian beam prestack depth migration (GB-PSDM) method is presented in this paper. Unlike the method of Zhu et al. (2007), the anisotropic kinematic and dynamic ray tracing in our migration method are not formulated in terms of phase velocity and group velocity. The purpose of this study is to provide an accurate migration method for P-wave data in TI media. Detailed analyses on different TI media models and field seismic data are carried out, using isotropic and anisotropic GB-PSDM respectively, to verify the accuracy and effectiveness of this method.

The elastic parameters of the TI media

The character of the TI media is determined by the stiffness matrix $\boldsymbol{C}$, which is used to express the stress–strain relations. The stiffness matrix of TI media has five independent elastic constants. The one with a vertical symmetry-axis (vertical transversely isotropic, VTI) is given by (Tsvankin, 2005)

$$\boldsymbol{C}=\begin{bmatrix} c_{11} & c_{11}-2c_{66} & c_{13} & 0 & 0 & 0 \\ c_{11}-2c_{66} & c_{11} & c_{13} & 0 & 0 & 0 \\ c_{13} & c_{13} & c_{33} & 0 & 0 & 0 \\ 0 & 0 & 0 & c_{44} & 0 & 0 \\ 0 & 0 & 0 & 0 & c_{44} & 0 \\ 0 & 0 & 0 & 0 & 0 & c_{66} \end{bmatrix} \tag{1}$$

As the physical meaning of elastic constants is not straightforward, Thomsen (1986) introduced a set of parameters to describe anisotropy, which facilitate the research of the anisotropic media and better show the physical meaning of anisotropic parameters. The Thomsen's parameters are defined by the elastic constants of VTI media as

$$V_{P0}=\sqrt{\frac{c_{33}}{\rho}},\ V_{S0}=\sqrt{\frac{c_{55}}{\rho}},\ \varepsilon=\frac{c_{11}-c_{33}}{2c_{33}},\\ \gamma=\frac{c_{66}-c_{44}}{2c_{44}},\ \delta=\frac{(c_{13}+c_{44})^2-(c_{33}-c_{44})^2}{2c_{33}(c_{33}-c_{44})} \tag{2}$$

where ρ is density; V_{P0} and V_{S0} are phase velocities of P- and SV-waves along the symmetry-axis of VTI media, respectively; ε δ and γ are three dimensionless anisotropic parameters, which characterise the magnitude of anisotropy. The parameters ε and γ represent the anisotropy of P- and SH-waves, respectively. The parameter δ governs the P-wave velocity variation away from the symmetry-axis and also influences the SV-wave velocity (Tsvankin et al., 2010). According to the relationship between Thomsen's parameters and elastic constants, the elastic constants can be expressed with Thomsen's parameters as

$$c_{11}=\rho(1+2\varepsilon)V_{P0}^2,\quad c_{33}=\rho V_{P0}^2,\\ c_{44}=c_{55}=\rho V_{S0}^2,\quad c_{66}=\rho(1+2\gamma)V_{S0}^2,\\ c_{13}=\sqrt{2\delta c_{33}\,(c_{33}-c_{44})+(c_{33}-c_{44})^2}-c_{44} \tag{3}$$

When elastic boundaries in the subsurface are dipping, the symmetry-axis of TI media may not be vertical. Such media are referred to as TI media with a tilted symmetry-axis (tilted transversely isotropic, TTI). In this paper, the angle between symmetry-axis and vertical direction is denoted as θ for TTI media. The stiffness matrix of TTI media can be obtained from the stiffness matrix of VTI media with Bond transformation (Winterstein, 1990).

GB-PSDM in anisotropic media

The image of anisotropic GB-PSDM is formed by cross-correlating the downward-continued wavefields from source and beam centres, which is the same as GB-PSDM in isotropic media. The extension of Gaussian beam migration to anisotropic media requires calculation of the complex-valued time and amplitude using anisotropic kinematic and dynamic ray tracing. Therefore, the key of anisotropic GB-PSDM is anisotropic kinematic and dynamic ray tracing.

Prestack migration theory

According to the Gaussian beam prestack migration method that operates on common-offset gathers given by Hill (2001), GB-PSDM formula of common-shot records in two-dimensional media can be written as

$$I(\mathbf{x})=C\int dx_s\sum_{\mathbf{L}_r}\int d\omega\int dp_{sx}\int dp_{rx}u^*_{GB}\,(\mathbf{x},\ \mathbf{x}_s,\ \mathbf{p}_s,\ \omega)\\ u^*_{GB}(\mathbf{x},\ \mathbf{L}_r,\ \mathbf{p}_r,\ \omega)\ \mathbf{D}\,(\mathbf{L}_r,\ \mathbf{p}_r,\ \omega) \tag{4}$$

where $I(\mathbf{x})$ is the final image at subsurface point $\mathbf{x}$, ω is circular frequency and C denotes corresponding constant. $u^*_{GB}(\mathbf{x}, \mathbf{x}_s, \mathbf{p}_s, \omega)$ and $u^*_{\mathrm{GB}}(\mathbf{x}, \mathbf{L}_r, \mathbf{p}_r, \omega)$ are the complex conjugates of the normalised Gaussian beam solutions to the wave equation (Hill, 2001), where the former represents wave propagation from source $\mathbf{x}_s$ with initial direction $\mathbf{p}_s$, and the latter represents wave propagation from the beam centre $\mathbf{L}_r$ with initial direction $\mathbf{p}_r$. $D(\mathbf{L}_r, \mathbf{p}_r, \omega)$ is the local plane wave component obtained from a local slant stack of the common-shot traces, and the expression can be written as (Hill, 2001; Gray and Bleistein, 2009)

$$D(\mathbf{L}_r,\ \mathbf{p}_r,\ \omega)=\frac{1}{4\pi^2}\left|\frac{\omega}{\omega_r}\right|^3\int dx_r u(\mathbf{x}_r,\ \mathbf{x}_s,\omega)\\ \times\exp\left[-i\omega\mathbf{p}_r\,(\mathbf{x}_r-\mathbf{L}_r)-\frac{1}{2}\left|\frac{\omega}{\omega_r}\right|\frac{|\mathbf{x}_r-\mathbf{L}_r|^2}{L_0^2}\right] \tag{5}$$

where ω_r is reference frequency and $u(\mathbf{x}_r, \mathbf{x}_s, \omega)$ is the recorded wavefield. $L_0=\frac{v_{avg}}{f_{min}}$ is the initial beam width, where f_{min} is the minimum frequency and v_{avg} is the average of the horizontal and vertical velocities over the entire grid (Alkhalifah, 1995).

Central rays with different ray parameters are emitted from source and beam centers to compute wavefields for GB-PSDM, so it must have adequate ray coverage to guarantee the accuracy of migration imaging. The values of the minimum ray parameter P_{min} and the maximum ray parameter P_{max} in anisotropic media are different from those in isotropic media, given the same minimum and maximum angles and the same vertical velocity. Therefore, in order to get enough ray coverage, Alkhalifah (1995) modified the ray parameter spacing expression in isotropic media and presented the following expression adapted to anisotropic GB-PSDM

$$\Delta p_x=(\Delta p_x)_{iso}\frac{2v_{min}}{V_{min}(p_{max})+V_{min}(p_{min})} \tag{6}$$

where v_{min} is the minimum vertical velocity at the surface; V_{min} (P_{max}) and V_{min} (p_{min}) are the phase velocities corresponding to the maximum and minimum ray parameters, respectively, at the point $V_p=v_{min}$ on the surface. $(\Delta p_x)_{iso}$ is the ray parameter spacing for isotropic Gaussian beam migration (Hale, 1992*a*), given by

$$(\Delta p_x)_{iso}=\frac{\pi}{3L_0\sqrt{|\omega_l\omega_h|}} \tag{7}$$

where ω_l is the lowest circular frequency, ω_h is the highest circular frequency and L_0 is the related initial beam width.

Anisotropic kinematic ray tracing

Based on the anisotropic ray tracing theory derived by Červeny (1972, 2001), the kinematic ray tracing system of P-waves in two-dimensional TI media can be written as

$$\frac{dx_1}{d\tau}=a_{11}p_1g_1g_1+a_{15}p_3g_1g_1+2a_{15}p_1g_1g_3+a_{13}p_3g_1g_3\\ +a_{55}p_3g_1g_3+a_{55}p_1g_3g_3+a_{35}p_3g_3g_3 \tag{8}$$

$$\frac{dx_3}{d\tau}=a_{15}p_1g_1g_1+a_{55}p_3g_1g_1+a_{55}p_1g_1g_3+2a_{35}p_3g_1g_3\\ +a_{13}p_1g_1g_3+a_{35}p_1g_3g_3+a_{33}p_3g_3g_3 \tag{9}$$

$$\frac{dp_1}{d\tau} = -\frac{1}{2}\left(\frac{\partial a_{11}}{\partial x_1}p_1p_1g_1g_1 + 2\frac{\partial a_{15}}{\partial x_1}p_1p_3g_1g_1 + 2\frac{\partial a_{15}}{\partial x_1}p_1p_1g_1g_3 + 2\frac{\partial a_{13}}{\partial x_1}p_1p_3g_1g_3 + 2\frac{\partial a_{55}}{\partial x_1}p_1p_3g_1g_3 + \frac{\partial a_{55}}{\partial x_1}p_1p_1g_3g_3 + 2\frac{\partial a_{35}}{\partial x_1}p_1p_3g_3g_3 + \frac{\partial a_{55}}{\partial x_1}p_3p_3g_1g_1 + 2\frac{\partial a_{35}}{\partial x_1}p_3p_3g_1g_3 + \frac{\partial a_{33}}{\partial x_1}p_3p_3g_3g_3\right) \quad (10)$$

$$\frac{dp_3}{d\tau} = -\frac{1}{2}\left(\frac{\partial a_{11}}{\partial x_3}p_1p_1g_1g_1 + 2\frac{\partial a_{15}}{\partial x_3}p_1p_3g_1g_1 + 2\frac{\partial a_{15}}{\partial x_3}p_1p_1g_1g_3 + 2\frac{\partial a_{13}}{\partial x_3}p_1p_3g_1g_3 + 2\frac{\partial a_{55}}{\partial x_3}p_1p_3g_1g_3 + \frac{\partial a_{55}}{\partial x_3}p_1p_1g_3g_3 + 2\frac{\partial a_{35}}{\partial x_3}p_1p_3g_3g_3 + \frac{\partial a_{55}}{\partial x_3}p_3p_3g_1g_1 + 2\frac{\partial a_{35}}{\partial x_3}p_3p_3g_1g_3 + \frac{\partial a_{33}}{\partial x_3}p_3p_3g_3g_3\right) \quad (11)$$

where $p_i = \frac{\partial \tau}{\partial x_i}$ are the components of the phase vector, $a_{mn} = c_{mn}/\rho$ are the density-normalised elastic parameters, and g_j are the components of the eigenvector for the Christoffel matrix Γ. The product of eigenvectors are given by (Alkhalifah, 1995)

$$g_1g_1 = \frac{\Gamma_{33} - 1}{\Gamma_{11} + \Gamma_{33} - 2},$$
$$g_3g_3 = \frac{\Gamma_{11} - 1}{\Gamma_{11} + \Gamma_{33} - 2}, \quad (12)$$
$$g_1g_3 = \frac{-\Gamma_{13}}{\Gamma_{11} + \Gamma_{33} - 2}$$

The Christoffel matrix $\Gamma_{ik} = a_{ijkl}p_jp_l$ contains the components of slowness vector (Červeny, 2001), which has been broadly used in the ray method of seismic waves propagating in inhomogeneous anisotropic media, as it is very suitable for the study of the ray method.

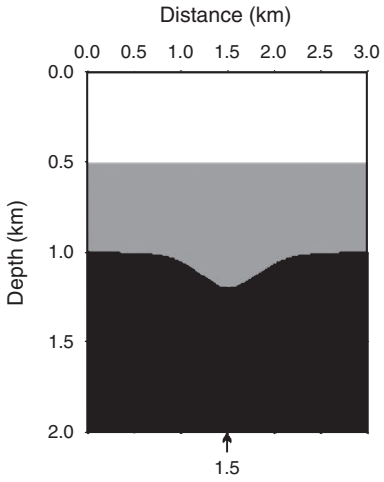

Fig. 1. Subsurface tilted transversely isotropic (TTI) media model with different anisotropy parameters in each layer. The middle layer is a TTI medium with the symmetry-axis dipping at 60°.

Table 1. Anisotropic parameters of the tilted transversely isotropic (TTI) syncline model.

Layer	V_{P0} (m/s)	ε	δ	θ
1	2400	0.12	0.08	0°
2	2800	0.18	0.1	60°
3	3200	0.0	0.0	0°

Anisotropic dynamic ray tracing

For anisotropic media, the ray-centred coordinates are no longer orthogonal as they are in isotropic media. The wavefield energy does not propagate in the direction of the phase-velocity vector and the rays are not perpendicular to wavefronts. So the dynamic ray tracing is more complicated in anisotropic media, and the expression can be written as (Hanyga, 1986; Alkhalifah, 1995)

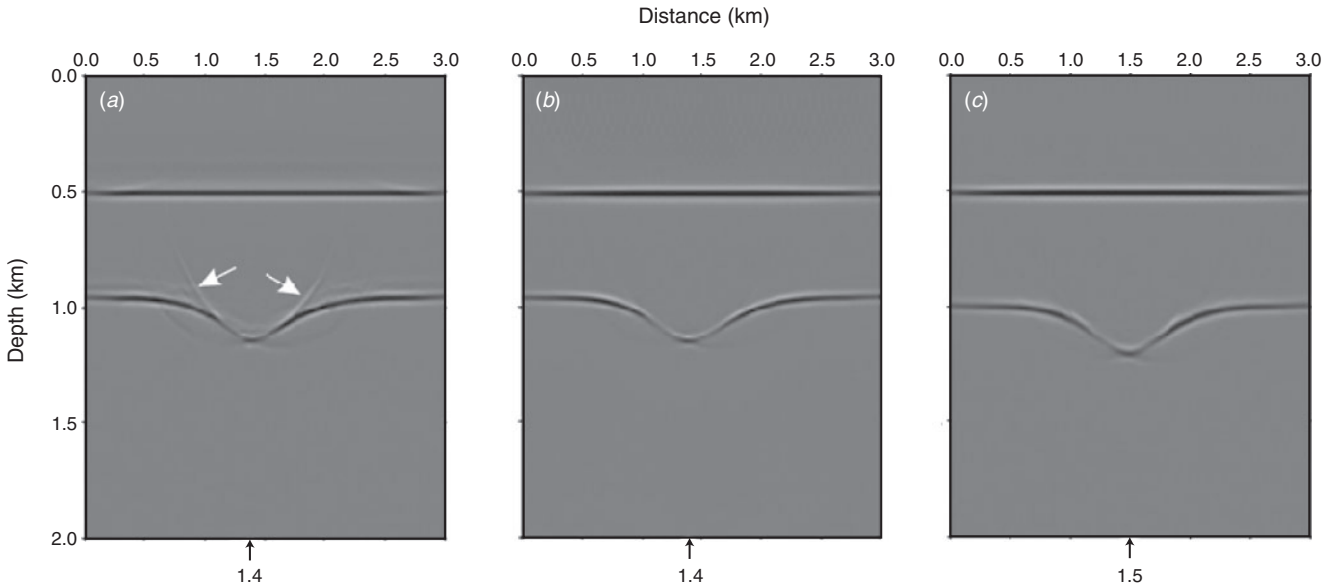

Fig. 2. (*a*) Isotropic Gaussian beam prestack depth migration (GB-PSDM) result without considering the effect of anisotropy. The synclinal structure is mispositioned in both vertical and horizontal directions. Defocusing artefacts are visible around the synclinal structure, as shown by the arrow. (*b*) Anisotropic GB-PSDM result without taking the symmetry-axis tilt in the middle layer into account. The noise and defocusing artefacts are eliminated, but the synclinal structure is also not imaged at the correct position. (*c*) Anisotropic GB-PSDM result with the true model parameters. The model has been accurately imaged. The defocusing artefacts around the synclinal structure are also eliminated.

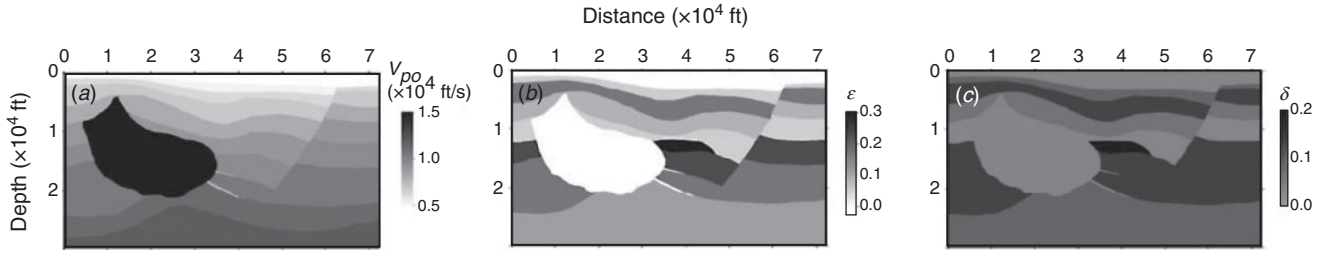

Fig. 3. The vertical velocity and anisotropy parameters for the synthetic data: (*a*) vertical velocity V_{P0}; (*b*) anisotropy parameter ε; (*c*) anisotropy parameter δ.

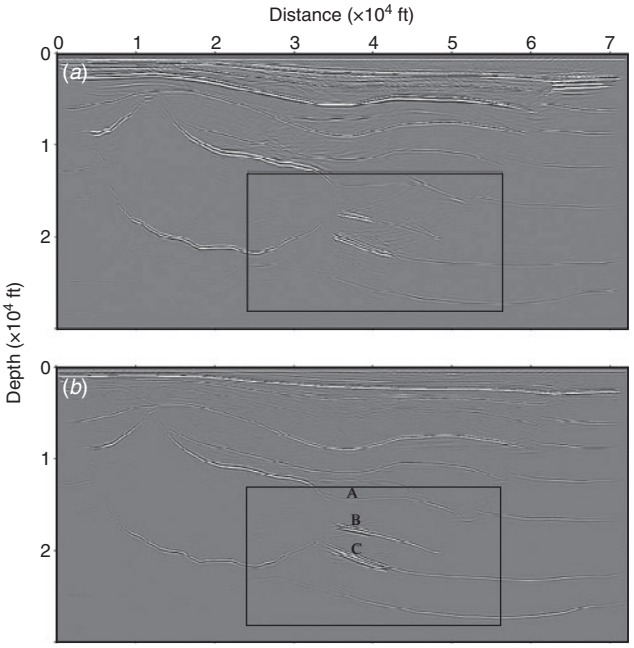

Fig. 4. Gaussian beam prestack depth migration (GB-PSDM) results: (*a*) isotropic migration; (*b*) anisotropic migration. The rectangular boxes in this figure marks the local magnification region to show the comparison of images more clearly.

$$\begin{cases} \dfrac{dq}{d\tau} = Mp + Vq \\ \dfrac{dq}{d\tau} = -Vp - Hq. \end{cases} \tag{13}$$

where M, V, H are derivatives of G_m with respect to n and P_n, given by

$$M = 0.5\frac{\partial^2 G_m}{\partial n^2} - 0.25\left(\frac{\partial G_m}{\partial n}\right)^2,$$
$$H = 0.5\frac{\partial^2 G_m}{\partial p_n^2} - 0.25\left(\frac{\partial G_m}{\partial p_n}\right)^2, \tag{14}$$
$$V = 0.5\frac{\partial^2 G_m}{\partial p_n \partial n} - 0.25\frac{\partial G_m}{\partial p_n}\frac{\partial G_m}{\partial n}$$

where P_n is the ray parameter in the direction of n, which is perpendicular to the wavefront. G_m are the eigenvalues of the Christoffel equation, and

$$G_m = a_{ijkl}\, p_j\, p_l g_i^{(m)} g_k^{(m)} \tag{15}$$

where G_m ($m = 1, 2, 3$) are the three eigenvalues representing the eikonal equation for the three wave types (Červeny, 2001).

Numerical examples

Syncline model

Some previous papers have shown how anisotropic parameters ε and δ affect image quality (Alkhalifah and Larner, 1994; Vestrum et al., 1999). In this section, a TTI syncline model is used to demonstrate the accuracy of the anisotropic GB-PSDM method and investigate the influence of tilt angle on migration. The model contains three layers with different anisotropic parameters, and the middle layer is TTI media, as shown in Figure 1. The specific anisotropic parameters of the model are shown in Table 1. The P-wave synthetic dataset is generated using anisotropic ray tracing forward modelling method, and the source wavelet is the Ricker wavelet with a dominant frequency of 30 Hz. A total of 41 shots are acquired on the surface with 321 receivers per shot. The shot spacing is 70 m and the receiver spacing is 10 m. The traveltime is 1.6s with 2 ms sampling.

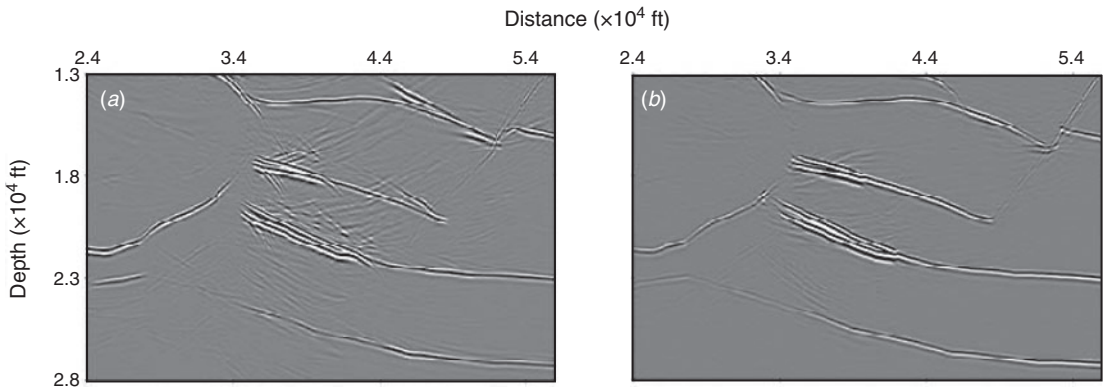

Fig. 5. Comparisons of local magnification between (*a*) isotropic and (*b*) anisotropic prestack depth migration results. Clearly the image in Figure 5*b* is superior to that in Figure 5*a*. Anisotropic migration provides correct images of the lens and steep fault. The noise is eliminated and the breakpoint is clear in Figure 5*b*.

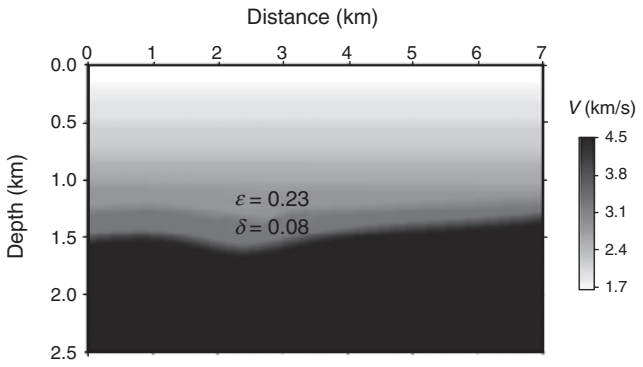

Fig. 6. Velocity model for the field data example. Only the layers in the middle of the model are considered anisotropic with Thomsen parameters $\varepsilon = 0.23$ and $\delta = 0.08$.

Figure 2*a* displays the resulting image using the isotropic GB-PSDM algorithm with the velocity $V_P = V_{P0}$, where the image of the synclinal structure has large position error in both the vertical and horizontal directions. The noise is serious near the reflection interface, and defocusing artefacts are obvious around the synclinal structure, as shown by the arrow in Figure 2*a*. As a comparison, the image using the anisotropic GB-PSDM method with a tilt angle θ in the middle layer given as zero is shown in Figure 2*b*. The noise and defocusing artefacts are eliminated, but the synclinal structure is not imaged at the correct position because of the ignoring of the tilt angle. In the above two migrations, the vertical velocities are less than the true vertical velocity in the TTI layer, which causes the vertical upward shift of the imaged synclinal structure. In addition, as the horizontal velocities are incorrect for the TTI layer, the imaged synclinal structure also has a lateral shift. This mispositioning caused by overburden TTI media has also been described with synthetic data (e.g. Zhang et al., 2004; Du et al., 2007; Behera and Tsvankin, 2009). In contrast, the image from anisotropic GB-PSDM with the true model parameters (Figure 2*c*) shows an accurate image of the synclinal structure, and the defocusing artefacts are also eliminated. The test results show that using our anisotropic GB-PSDM can get an accurate image for TTI media. The results also show that the tilt angle θ has a significant influence on the accuracy of migrated image in TTI media and ignoring the influence of tilt angle may lead to obvious image errors.

SEG/Hess VTI model

The anisotropic GB-PSDM method is further tested using a SEG/Hess VTI model. Figure 3*a* shows the vertical velocity of the Hess VTI model. Figure 3*b*, *c* depicts the anisotropic parameters ε and δ of the model, respectively. The synthetic dataset is generated using the finite-difference forward modelling method in VTI media. A total of 720 shots are acquired with a shot spacing of 100ft, and the receiver spacing is 40ft. The minimum offset for each shot is 0 ft, and the maximum offset is 26200 ft. The trace length is 7.992 s with 6 ms sampling. Both vertical and horizontal spacing of anisotropic parameters are 20 ft.

Figure 4 shows images of the Hess VTI synthetic dataset using (a) isotropic GB-PSDM and (b) anisotropic GB-PSDM in VTI media. In order to present the comparison more clearly, the images of rectangular boxes in Figure 4 are magnified. Figure 5*a* shows the isotropic imaging result and Figure 5*b* shows the anisotropic imaging result. The image from the isotropic migration, which ignores the influence of anisotropy, shows that the image of a salt dome located on the left side of the model is not accurate, the lens A in the middle of the model is not imaged, and images of the lenses B and C are mixed and disorderly. The imaging position of a steep fault located on the right side of the model is not accurate, in either the vertical or horizontal direction, and the noise is serious on the migrated section. In contrast, the image from our anisotropic GB-PSDM shows that the salt dome is imaged at the correct position and the lenses A, B and C are all well imaged. The imaging position of the steep fault is accurate and the breakpoint is clear. It can be seen clearly that the image from the anisotropic migration is superior to the image from the isotropic migration.

Field data example

To demonstrate the applicability of the method, we apply it to a field seismic dataset acquired in north-eastern China. The total amount of data is 36 000 traces and the trace spacing is 10 m. The recording length is 2 s with a sampling interval of 1 ms. A section of the derived velocity model is shown in Figure 6. Only the layers in the middle of the model are considered to be anisotropic, and the values of anisotropic parameters ε and σ are given in the velocity model, as shown in Figure 6. Figure 7*a*, *b* shows the resulting images of the field data using isotropic and anisotropic GB-PSDM, respectively. Differences observed between the images are attributed only to differences between the isotropic and anisotropic migrations. The rectangular boxes in Figure 7

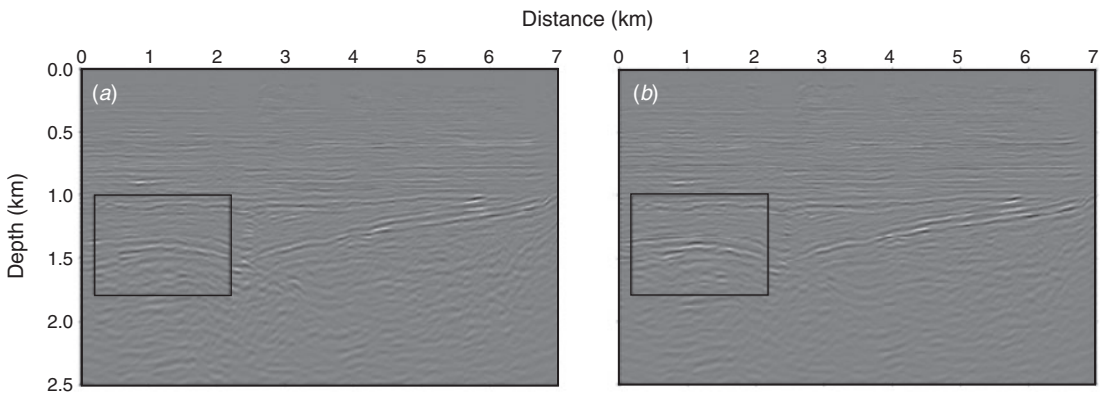

Fig. 7. The resulting images of the field data: (*a*) isotropic Gaussian beam prestack depth migration (GB-PSDM); (*b*) anisotropic GB-PSDM. The rectangular boxes on both sections mark the local magnification regions, where some of the key improvements of anisotropic migration when compared to isotropic migration are highlighted.

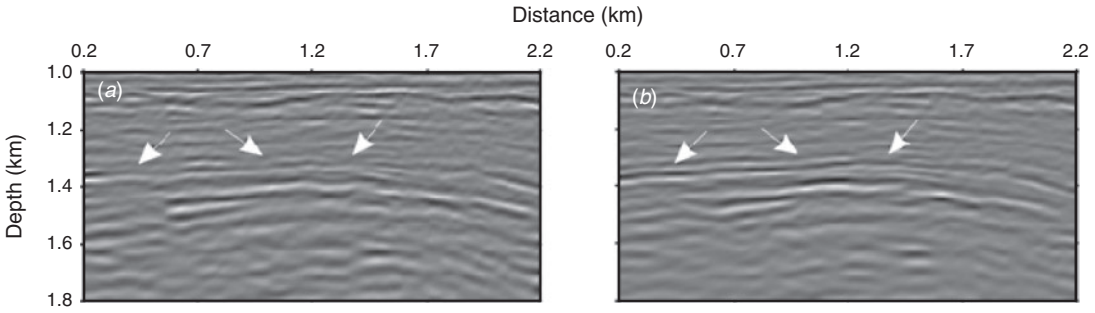

Fig. 8. Comparisons of local magnification between (*a*) isotropic and (*b*) anisotropic prestack depth migration results. The arrows point to the main improvements achieved by taking anisotropy into account. A better focus imaging for target layer is provided by anisotropic migration.

highlight some of the key improvements of anisotropic depth migration, and the images of the boxes are magnified. Figure 8*a*, *b* shows the local magnification of isotropic and anisotropic prestack depth migration results. Seeing the target layer indicated by the arrows, better focus imaging is provided by the anisotropic migration. It can be seen clearly that the image quality is improved using anisotropic depth migration. The test results demonstrate that our anisotropic GB-PSDM method is applicable and efficient.

Conclusions

Based on the study of Gaussian beam poststack depth migration for anisotropic media, an anisotropic GB-PSDM method for P-wave data in TI media is presented in this paper. The key of this method is anisotropic kinematic and dynamic ray tracing. The method takes the influence of anisotropy on seismic waves into account, and can obtain accurate seismic images of subsurface structures in anisotropic media. Meanwhile, it retains the capability of the isotropic GB-PSDM method to image multipathing arrivals and steeply dipping structures. Tests of synthetic and field seismic data demonstrate that the method introduced above is an accurate and efficient anisotropic prestack depth migration method in TI media. Also, tests of the TTI media model show that the tilt angle has a significant influence on the accuracy of the migrated image in TTI media and ignoring the influence of the tilt angle may lead to obvious vertical and horizontal mispositioning.

Acknowledgements

The authors would like to thank the Hess Corporation for making the Hess VTI dataset publicly available. This research was supported by the National Special Fund of China (grant no. 2011ZX05035–001–006HZ, 008–006–22, 049–01–02, 019–003) and the National 863 Program of China (grant no. 2013AA064201).

References

Alkhalifah, T., 1995, Gaussian beam depth migration for anisotropic media: *Geophysics*, **60**, 1474–1484. doi:10.1190/1.1443881

Alkhalifah, T., and Larner, K., 1994, Migration errors in transversely isotropic media: *Geophysics*, **59**, 1405–1418. doi:10.1190/1.1443698

Ball, G., 1995, Estimation of anisotropy and anisotropic 3D prestack depth migration, offshore Zaire: *Geophysics*, **60**, 1495–1513. doi:10.1190/1.1443883

Behera, L., and Tsvankin, I., 2009, Migration velocity analysis for tilted transversely isotropic media: *Geophysical Prospecting*, **57**, 13–26. doi:10.1111/j.1365-2478.2008.00732.x

Červeny, V., 1972, Seismic rays and ray intensities in inhomogeneous anisotropic media: *Geophysical Journal International*, **29**, 1–13. doi:10.1111/j.1365-246X.1972.tb06147.x

Červeny, V. 2001, *Seismic ray theory*: Cambridge University Press.

Du, X., Bancroft, J. C., and Lines, L. R., 2007, Anisotropic reverse-time migration for tilted TI media: *Geophysical Prospecting*, **55**, 853–869. doi:10.1111/j.1365-2478.2007.00652.x

Gray, S. H., 2005, Gaussian beam migration of common-shot records: *Geophysics*, **70**, S71–S77. doi:10.1190/1.1988186

Gray, S. H., and Bleistein, N., 2009, True-amplitude Gaussian-beam migration: *Geophysics*, **74**, S11–S23. doi:10.1190/1.3052116

Hale, D., 1992*a*, Migration by the Kirchhoff, slant stack and Gaussian beam methods: Colorado School of Mines Center for Wave Phenomena Report 121.

Hale, D., 1992*b*, Computational aspects of Gaussian beam migration: Colorado School of Mines Center for Wave Phenomena Report 139.

Hanyga, A., 1986, Gaussian beams in anisotropic elastic media: *Geophysical Journal International*, **85**, 473–504. doi:10.1111/j.1365-246X.1986.tb04528.x

Hill, N. R., 1990, Gaussian beam migration: *Geophysics*, **55**, 1416–1428. doi:10.1190/1.1442788

Hill, N. R., 2001, Prestack Gaussian-beam depth migration: *Geophysics*, **66**, 1240–1250. doi:10.1190/1.1487071

Pedersen, Ø., Ursin, B., and Helgesen, H. K., 2010, One-way wave-equation migration of compressional and converted waves in a VTI medium: *Geophysics*, **75**, S237–S248. doi:10.1190/1.3509466

Popov, M. M., Semtchenok, N. M., Popov, P. M., and Verdel, A. R., 2008, Reverse time migration with Gaussian beams and velocity analysis applications: 70th Annual International Meeting, EAGE, Extended Abstracts, F048.

Popov, M. M., Semtchenok, N. M., Popov, P. M., and Verdel, A. R., 2010, Depth migration by the Gaussian beam summation method: *Geophysics*, **75**, S81–S93. doi:10.1190/1.3361651

Thomsen, L., 1986, Weak elastic anisotropy: *Geophysics*, **51**, 1954–1966. doi:10.1190/1.1442051

Tsvankin, I., 2005, *Seismic signatures and analysis of reflection data in anisotropic media* (2nd edition): Elsevier Science Publ. Co., Inc.

Tsvankin, I., Gaiser, J., Grechka, V., Baan, M. V. D., and Thomsen, L., 2010, Seismic anisotropy in exploration and reservoir characterization: an overview: *Geophysics*, **75**, A15–A29. doi:10.1190/1.3481775

Vestrum, R. W., Lawton, D. C., and Schmid, R., 1999, Imaging structures below dipping TI media: *Geophysics*, **64**, 1239–1246. doi:10.1190/1.1444630

Wang, Z. J., 2002, Seismic anisotropy in sedimentary rocks, part 2: laboratory data: *Geophysics*, **67**, 1423–1440. doi:10.1190/1.1512743

Winterstein, D. F., 1990, Velocity anisotropy terminology for geophysicists: *Geophysics*, **55**, 1070–1088. doi:10.1190/1.1442919

Zhang, J. F., Verschuur, D. J., and Wapenaar, C. P. A., 2001, Depth migration of shot records in heterogeneous, transversely isotropic media using optimum explicit operators: *Geophysical Prospecting*, **49**, 287–299. doi:10.1046/j.1365-2478.2001.00255.x

Zhang, L. B., Rector, J. W. III, and Hoversten, G. M., 2004, Reverse time migration in tilted transversely isotropic media: *Journal of Seismic Exploration*, **13**, 173–188.

Zhu, T. F., Gray, S. H., and Wang, D. L., 2007, Prestack Gaussian-beam depth migration in anisotropic media: *Geophysics*, **72**, S133–S138. doi:10.1190/1.2711423